Biochimica et Biophysica Acta 1778 (2008) 2480-2486

Contents lists available at ScienceDirect

Biochimica et Biophysica Acta

journal homepage: www.elsevier.com/locate/bbamem

Line tension at lipid phase boundaries regulates formation of membrane vesicles in living cells

Dina Vind-Kezunovic [a,*,1], Claus Hélix Nielsen [b,1], Urszula Wojewodzka [c], Robert Gniadecki [a]

[a] Department of Dermatology, Copenhagen University Hospital, Bispebjerg, DK-2400 Copenhagen NV, Denmark
[b] Quantum Protein Centre, Department of Physics, Technical University of Denmark, DK-2800 Kgs. Lyngby, Denmark
[c] Department of Cell Ultrastructure, Polish Academy of Sciences Medical Research Center, 02-106 Warsaw, Poland

ARTICLE INFO

Article history:
Received 23 January 2008
Received in revised form 8 May 2008
Accepted 23 May 2008
Available online 10 June 2008

Keywords:
Domain formation
Line tension
Plasma membrane
Vesiculation

ABSTRACT

Ternary lipid compositions in model membranes segregate into large-scale liquid-ordered (L_o) and liquid-disordered (L_d) phases. Here, we show μm-sized lipid domain separation leading to vesicle formation in unperturbed human HaCaT keratinocytes. Budding vesicles in the apical portion of the plasma membrane were predominantly labelled with L_d markers 1,1′-dioctadecyl-3,3,3′,3′-tetramethylindocarbocyanine perchlorate, 1,1′-dilinoleyl-3,3,3′,3′-tetramethylindocarbocyanine perchlorate, 1,1′-didodecyl-3,3,3′,3′-tetramethylindocarbocyanine perchlorate and weakly stained by L_o marker fluorescein-labeled cholera toxin B subunit which labels ganglioside GM_1 enriched plasma membrane rafts. Cholesterol depletion with methyl-β-cyclodextrin enhanced DiI vesiculation, GM_1/DiI domain separation and was accompanied by a detachment of the subcortical cytoskeleton from the plasma membrane. Based on these observations we describe the energetic requirements for plasma membrane vesiculation. We propose that the decrease in total 'L_o/L_d' boundary line tension arising from the coalescence of smaller L_d-like domains makes it energetically favourable for L_d-like domains to bend from flat μm-sized surfaces to cap-like budding vesicles. Thus living cells may utilize membrane line tension energies as a control mechanism of exocytic events.

1. Introduction

Plasma membranes are heterogeneously organized into dynamic sphingolipid and cholesterol enriched assemblies that are thought to be analogous to liquid-ordered (L_o) domains seen in model membranes (for a review, see [1]). In giant unilamellar vesicles (GUVs) μm-sized liquid-ordered (L_o) phases form with a lipid composition mimicking the outer leaflet of the plasma membrane [2], whereas domains in living cells are of nm-size [3]. A likely reason for this discrepancy is that the plasma membrane contains trans-membrane proteins anchored to the cytoskeleton [4]. Another reason may reside in the fact that the plasma membrane lipid composition is poised for phase separation upon release from the underlying cytoskeleton and subsequent endocytic/exocytic processes [5].

Studies on model systems suggest that domain formation occurs as a consequence of L_o/L_d lipid phase immiscibility [2]. L_o and L_d phases differ in transition temperature, bending modulus κ, and thickness [6]. Consequently, a line tension arises at the edge of the L_o/L_d boundary, and it has been suggested that the phase separation minimizes the total line tension by vesicle formation [7], Many mechanisms have been proposed to drive vesiculation [8]. Whether line tension plays a role in this process is unclear.

In GUVs, long-range L_o/L_d phase separation drives vesicle formation based on the two phases' different abilities to curve [9], and L_d lipids accumulate within highly curved regions from which L_d tubule fission arises [10]. Tubule fission is enhanced in response to cholesterol depletion by methyl-β-cyclodextrin (MβCD) [10].

The likely role of cholesterol in allowing L_o phase formation has made cholesterol depletion by MβCD a well-established tool to study the L_o phase in cellular functions.

In GUVs the L_o phase can be marked with fluorescein isothiocyanate-tagged cholera toxin B subunit (CTB) [11]. The L_d phase can be marked with long acyl chain and saturated 1,1′-dioctadecyl-3,3,3′,3′-tetramethylindocarbocyanine perchlorate (DiI-$C_{18:0}$) [11,12], 1,1′-didodecyl-3,3,3′,3′-tetramethylindocarbocyanine perchlorate (DiI-$C_{12:0}$) which has a short DiI saturated tail [13] and di-unsaturated 1,1′-dilinoleyl-3,3,3′,3′-tetramethylindocarbocyanine perchlorate (DiI-$C_{18:2}$) [14,15].

Abbreviations: BSA, bovine serum albumin; CTB-FITC, cholera toxin B subunit-conjugated fluorescein isothiocyanate; DiI-$C_{12:0}$, 1,1′-didodecyl-3,3,3′,3′-tetramethylindocarbocyanine perchlorate; DiI-$C_{18:0}$, 1,1′-dioctadecyl-3,3,3′3′-tetramethylindocarbocyanine perchlorate; DiI-$C_{18:2}$, 1,1′-dilinoleyl-3,3,3′,3′-tetramethylindocarbocyanine perchlorate; DMEM, Dulbecco's modified Eagle's medium; EFEM, embedment-free electron microscopy; GFP, green fluorescent protein; GUV, giant unilamellar vesicle; L_d, liquid-disordered; L_o, liquid-ordered; MβCD, methyl-β-cyclodextrin; PBS, phosphate buffered saline; PH, pleckstrin homology; PIP_2, phosphatidylinositol 4,5-bisphosphate; PLC, phospholipase C; SEM, scanning electron microscopy; TEM, transmission electron microscopy

* Corresponding author: Tel.: +45 35316005; fax: +45 35316010.
E-mail address: dv01@bbh.regionh.dk (D. Vind-Kezunovic).
[1] These authors contributed equally to this work.

0005-2736/$ – see front matter © 2008 Elsevier B.V. All rights reserved.
doi:10.1016/j.bbamem.2008.05.015

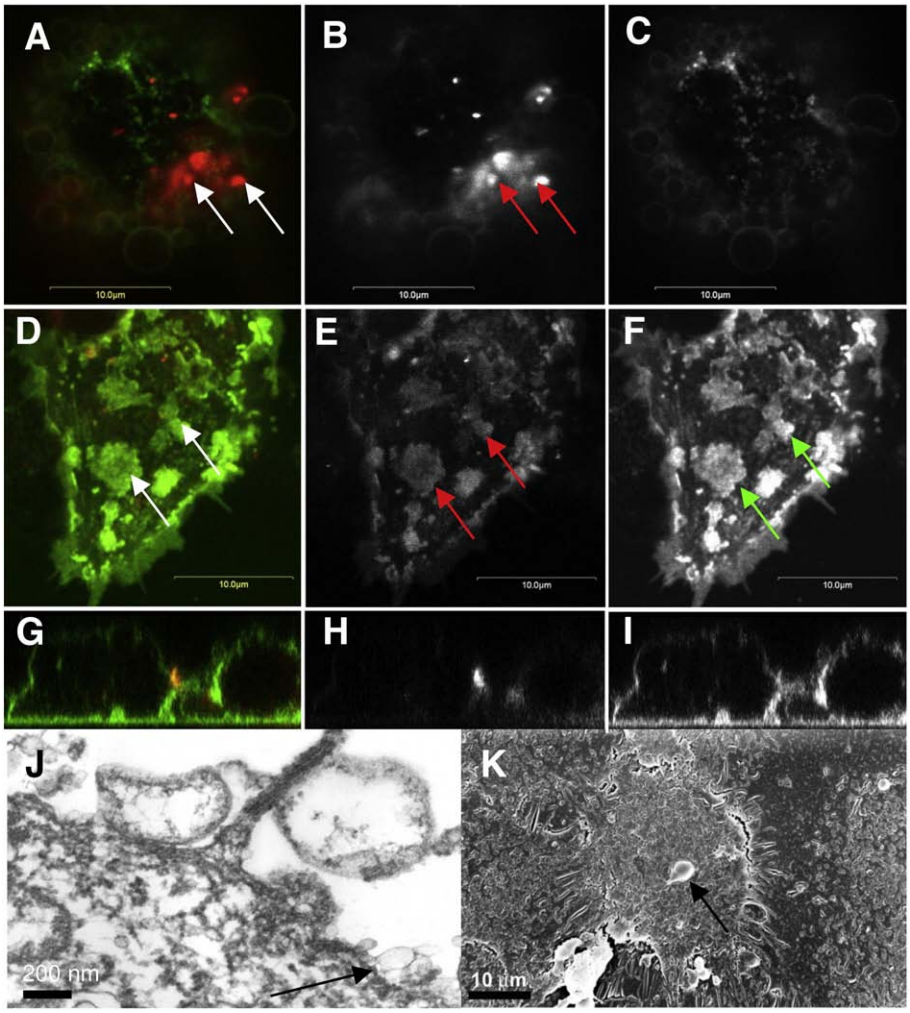

Fig. 1. Lipid domains and vesicle formation in intact HaCaT cells. Cells were stained with DiI-$C_{18:0}$ (30 min, 37 °C), washed in PBS, stained with CTB-FITC (30 min, RT) and imaged by confocal microscopy. (A) Merge of DiI-$C_{18:0}$ (red) and CTB-FITC (green), (B) DiI-$C_{18:0}$, (C) CTB-FITC. The corresponding construction is shown in D–I. Sections show the apical portion of the cell (A–C) and the basal portion of the cell (D–F). The *z*-plane reconstruction is shown in (G–I). Note the apical fission of vesicles stained with DiI-$C_{18:0}$ alone (arrows A, B) in contrast to the basal portion characterized by GM_1/DiI-$C_{18:0}$ domain overlap (arrows) (D–F). Scale bar, 10 μm. TEM (J) (bar, 200 nm) and SEM (K) (bar, 10 μm). Arrows show some vesicles.

The use of the positively charged DiI makes a direct comparison between GUV and cell studies difficult, and L_o and L_d phases are not well-defined entities in cells. Nevertheless, we believe that their use in biological membranes can shed light on potential phase based differences. Our recent measurements of fluorescence recovery by photobleaching (FRAP) revealed that cholesterol depletion by MβCD led to restricted molecular mobility in the basal portion of the plasma membrane due to coalescence of small GM_1 domains into larger micron-scale units [16]. In the apical part, we observed massive formation of 1–2 μm diameter sized vesicles stained with the L_d markers DiI-$C_{18:0}$, DiI-$C_{18:2}$ and DiI-$C_{12:0}$.

Lipowsky proposed a theoretical model, which predicts that an essentially flat domain can become unstable at a certain limiting size and then undergo a budding (or invagination) process. The line tension energy Γ can be reduced if many small domains coalesce into larger domains. The L_o phase has a larger κ and therefore it is favorable for the softer L_d phase to bulge out of the plasma membrane [7]. We hypothesized that vesicle formation was related to the line tension at the L_o/L_d boundary.

Here, we analyze vesicle formation. Our observations are consistent with predictions based on a continuum model. We show that Γ is sufficiently large to explain L_d vesiculation. We propose that separation of lipids on a μm-scale into 'L_d-like' and 'L_o-like' phases is a mechanism of membrane vesicle formation in living cells.

2. Materials and methods

2.1. Cell culture, transfection and fluorescence labelling for confocal microscopy

Immortalized human HaCaT keratinocytes [17] were cultured in Dulbecco's modified Eagle's medium (DMEM) supplemented with 10% heat-inactivated fetal calf serum (Gibco, Invitrogen) in a 5% humidified CO_2 incubator. Cholesterol was depleted by 1–2% MβCD (30 min, 37 °C) as described previously [16], 2% MβCD is 15.1 mM. For L_d phase labelling the cells were washed in phosphate buffered saline (PBS) and incubated with 1 μM DiI-$C_{18:0}$, 1.1 μM DiI-$C_{18:2}$ or 1.3 μM DiI-$C_{12:0}$ (Molecular Probes, Invitrogen) diluted in PBS or PBS containing 0.5% bovine serum albumin (BSA) for 30 min at 37 °C. CTB-FITC (Sigma) was used at a concentration of 2.5 μg/ml for 15 min at 4 °C or 30 min at room temperature. During confocal imaging cells were maintained in DMEM without phenol red (Gibco). Phosphatidylinositol 4,5-bisphosphate (PIP_2) enriched domains were visualized by the wild-type pleckstrin homology domain of phospholipase $C\delta_1$ tagged to a green fluorescent protein [18], in transiently transfected HaCaT cells as previously described [16]. F-actin filaments were labelled in paraformaldehyde-fixed, permeabilized cells (0.1% Triton X-100 in PBS, 5 min, 4 °C) with 5 U/ml Alexa Fluor 647 phalloidin (Invitrogen) for 20 min at 4 °C.

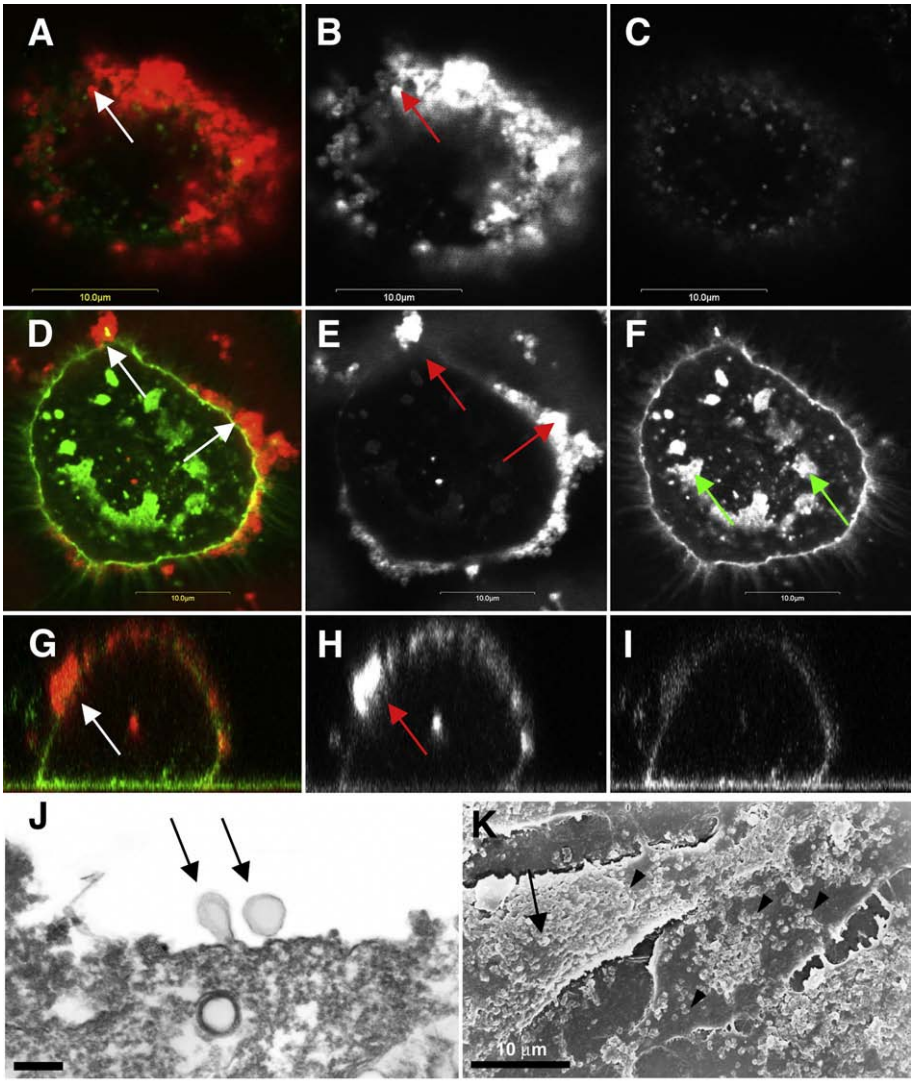

Fig. 2. Stimulation of vesiculation in HaCaT cells by MβCD. Cells were stained with DiI-$C_{18:0}$ as in Fig. 1, washed in PBS, and incubated with 2% MβCD for 30 min at 37 °C followed by staining with CTB-FITC (30 min, RT). (A) Merge of DiI-$C_{18:0}$ (red) and CTB-FITC (green), (B) DiI-$C_{18:0}$, (C) CTB-FITC. The corresponding construction is shown in D–I. Confocal images of the apical (A–C) and basal (D–F) portions and *z*-scan (G–I) of the cells were obtained as in Fig. 1. Scale bar, 10 µm. Note the DiI-$C_{18:0}$ vesicle formation (arrows) (A, B, D, E, G, H) and coalescence of GM_1 enriched domains by CTB (arrows, F). (J,K) The enhanced vesicle formation (arrows) was further confirmed by TEM (J) (bar, 200 nm) and SEM (K) (bar, 10 µm) on cholesterol-depleted cells (1% MβCD, 30 min, 37 °C).

Confocal images were obtained with the Olympus Fluoview confocal system built on the inverted IX70 microscope.

2.2. Electron microscopy

Cells were prepared for transmission electron microscopy (TEM) and scanning electron microscopy (SEM) according to standard protocol [19]. Embedment-free electron microscopy (EFEM) was performed according to the protocol of Nickerson [20] and modified for HaCaT cells [21,22]) using murine monoclonal antibodies against caveolin-2 (Becton-Dickinson, final dilution 1:100) and flotillin-2 (Becton-Dickinson, 1:20).

3. Results

3.1. Exocytic L_d vesicles and micron-scale GM_1/DiI-$C_{18:0}$ domain separation

Staining of cultured HaCaT cells with L_d marker DiI-$C_{18:0}$ [11,12,16] and CTB-fluorescein isothiocyanate (CTB-FITC), an L_o marker [23] unexpectedly revealed the presence of 1–2 µm diameter budding vesicles labelled mostly with DiI-$C_{18:0}$ (Fig. 1A). These vesicles were few and budded from the apical portion of the cell (Fig. 1B). The staining with CTB-FITC was weaker (Fig. 1C) and few overlaps between markers were observed in the apical portion (Fig. 1A). At the basal cell portion where membrane bending (and subsequent budding) is restricted due to glass attachment we observed an overlap (Fig. 1D) between DiI-$C_{18:0}$ (Fig. 1E) and GM_1 (Fig. 1F) within focal junctions [16]. To exclude artifactual phase separation due to GM_1 ganglioside cross-linking by pentameric CTB, we fixed cells with 4% paraformaldehyde after DiI-$C_{18:0}$ labelling but before CTB-FITC labelling and observed the same distribution (data not shown). Although paraformaldehyde cannot fix lipids, some fixation may take place because lipids may be linked to fixed proteins. Likewise, we saw DiI-$C_{18:0}$ labelled vesicles in living HaCaT cells stained solely with this dye (data not shown). TEM and SEM confirmed vesicle formation (Figs. 1J–K, arrows).

3.2. MβCD enhances GM_1/DiI-$C_{18:0}$ domain separation and vesiculation

Based on GUV studies we expected that cholesterol depletion would enhance the formation of L_d-like vesicles and this was observed

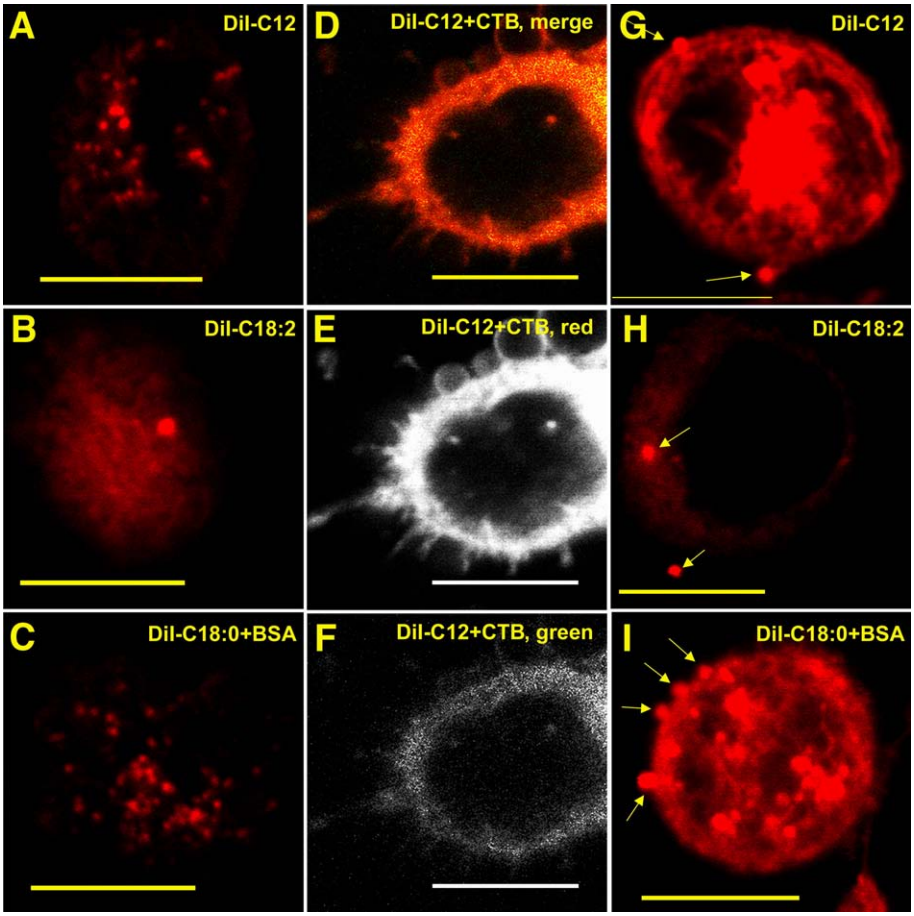

Fig. 3. Vesiculation of L_d marker DiI is not dependent on acyl chain length or saturation. (A, B) Cells were incubated with DiI-$C_{12:0}$ (A) or DiI-$C_{18:2}$ (B) diluted in PBS for 30 min at 37 °C, washed in PBS and imaged by confocal microscopy. (C) Cells were labelled with DiI-$C_{18:0}$ diluted in PBS containing 0.5% BSA (30 min, 37 °C), washed and imaged. Note DiI vesiculation in the apical portion of the cells. (D–F) Cells were incubated with DiI-$C_{12:0}$ as in A, washed in PBS, stained with CTB-FITC (15 min, 4 °C) and imaged by confocal microscopy. (D) Merge of DiI-$C_{12:0}$ (red) and CTB-FITC (green) in the apical cell portion, (E) DiI-$C_{18:0}$, (F) CTB-FITC. (G, H) Cells were labelled with DiI-$C_{12:0}$ and DiI-$C_{18:2}$ as in A, B, respectively and washed in PBS. After incubation with 2% MβCD (30 min, 37 °C), the apical cell portion was imaged showing DiI vesicles (arrows). (I) Cells were stained with DiI-$C_{18:0}$ as in C, washed in PBS, incubated with 2% MβCD (30 min, 37 °C) and imaged. Arrows show vesiculation of DiI-$C_{18:0}$ enriched vesicles. Bar, 10 μm.

(Figs. 2A, B). CTB staining was weak (Fig. 2C). At the basal membrane, MβCD induced μm-scale coalescence of L_o-like domains (Figs. 2D, F) with DiI-$C_{18:0}$ enriched vesicles budding off from the unattached membrane portion (Figs. 2E, G, H). We obtained similar data on MβCD-treated cells fixed in 4% paraformaldehyde before CTB-FITC labelling. We also observed enhanced DiI vesicle formation, when CTB-FITC staining was omitted. These findings were confirmed by TEM (Fig. 2J) and SEM (Fig. 2K).

3.3. Vesiculation of L_d marker DiI is not dependent on acyl chain length or saturation

Since 'L_d' is not a well-defined entity in cells, we have used other DiI probes, including the short tailed DiI, DiI-$C_{12:0}$ and the di-unsaturated DiI-$C_{18:2}$. DiI-$C_{12:0}$ preferentially partitions into the 'L_d' phase both in sphingomyelin/dioleoylphosphatidylcholine/cholesterol and distearoylphosphatidylcholine/dioleoylphosphatidylcholine/cholesterol model membrane (GUV) systems [13]. DiI-$C_{18:2}$ is a L_d marker in GUVs [15] and 'L_d-like' domain marker in cells [14]. Figs. 3A, B show spontaneous vesiculation with DiI-$C_{12:0}$ and DiI-$C_{18:2}$ markers, respectively in the apical cell portion of control cells. Securing uniform DiI staining in the absence of BSA is difficult, but when cells were stained with DiI-$C_{18:0}$ in the presence of 0.5% BSA vesiculation was still seen in control cells (Fig. 3C). In order to ensure that separation of DiI and CTB (induced by cross-linking) was not an endocytosis related phenomenon we performed CTB and DiI staining below 15 °C. Separation still occurred as shown in Figs. 3D–F for DiI-$C_{12:0}$ (similar results were obtained for DiI-$C_{18:0}$ and DiI-$C_{18:2}$, results not shown). Upon treatment with MβCD vesiculation was enhanced also using DiI-$C_{12:0}$ and DiI-$C_{18:2}$ markers (Figs. 3G, H). In the presence of 0.5% BSA, MβCD still enhanced vesiculation of DiI-$C_{18:0}$ as shown in Fig. 3I, and for DiI-$C_{12:0}$ and DiI-$C_{18:0}$, (results not shown).

3.4. MβCD disrupts the cortical cytoskeleton

Vesicle formation in living cells depends on loss of adhesion between the plasma membrane and the cytoskeleton (for a review, see [24]). We therefore speculated if cholesterol depletion and subsequent vesicle formation is accompanied by loss of adhesion. Although the linkage between the plasma membrane and the cytoskeleton is unclear, a pivotal role for the regulatory membrane phospholipid, PIP_2 has been proposed [25]. In accordance with an earlier study [26] we observed that cholesterol depletion with MβCD decreased the membrane content of green fluorescent protein pleckstrin homology domain of phospholipase Cδ_1 (GFP-PLCδ_1-PH) indicating a PIP_2-dependent reorganization of the cortical cytoskeleton (Figs. 4A, B). These findings were supported by phalloidin staining (Figs. 4C–F) and TEM (Figs. 4G, H) revealing that the

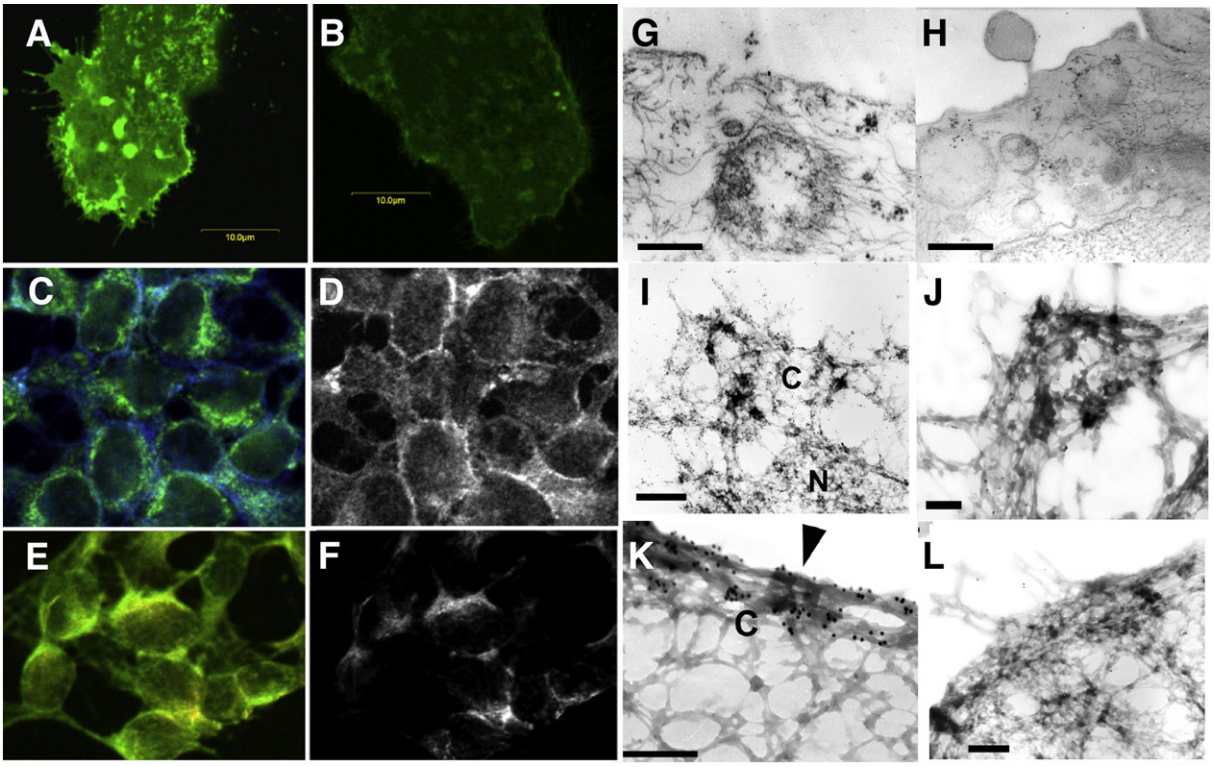

Fig. 4. MβCD induces loss of membrane–cytoskeleton adhesion. (A, B) HaCaT keratinocytes were transfected with wild-type PLCδ$_1$-PH-GFP, which binds to PIP$_2$. 24 h post-transfection, HaCaT cells were washed, incubated without (A) or with (B) 1% MβCD (30 min, 37 °C), washed and fixed in paraformaldehyde. Scale bar, 10 μm. (C–F) Confocal microscopy images of the plasma membrane labelled with CTB-FITC (green) and F-actin filaments labelled with phalloidin (blue); (D, F) depict the channel signal of phalloidin labelled F-actin. HaCaT cells were treated without (C, D) or with 2% MβCD (30 min, 37 °C) (E, F). Note that F-actin filaments are less abundant and disrupted in MβCD-treated cells (F) than in control cells (D). (G, H) Transmission electron micrographs comparing the structure of the cortical cytoskeleton of an intact HaCaT keratinocyte (G) with one treated with 2% MβCD (H). Note that in a control cell (G) networks of fine filaments extend throughout the cytoplasm and terminate at the plasma membrane whereas the fibrillar cytoplasmic actin meshwork is less dense after MβCD-treatment (H). (I–L) Embedment-free electron micrographs were labelled with L$_o$- and lipid raft markers flotillin 2 (I, K) and caveolin 2 (J, L), C = cytoskeleton and N = nucleus. (I, J) show the ultrastructure of the cytoskeleton in the vicinity of plasma membrane in unperturbed HaCaT cells. After MβCD-treatment the cortical cytoskeleton is flattened (K, L). Bar, 200 nm.

subcortical actin meshwork in MβCD-treated cells was disrupted. EFEM showed that the subcortical meshwork was reorganized and partially collapsed in cholesterol-depleted cells (Figs. 4I–L). We confirmed that the altered parts of the cytoskeleton were those immediately adjacent to the membrane by immunogold labelling of the membrane-associated proteins flotillin 2 and caveolin 2 (Figs. 4I–L).

3.5. Stimulated vesiculation is driven by line tension of DiI enriched vesicles

We considered the possibility that lipid phase separation and subcortical meshwork reorganization promote membrane bending and subsequently L$_d$-like vesiculation. Analysis of vesicle radius R and vesicle neck radius a from confocal images of 7 representative vesicles (Fig. 5A) revealed that $R = 0.90\ \mu m \pm 0.05\ \mu m$ and $a = 0.67\ \mu m \pm 0.06\ \mu m$ (mean ± standard error of the mean). As the L$_d$-like DiI budding vesicles were homogeneously sized and shaped with no apparent cytoskeletal attachments, we analyze vesiculation as an interplay between domain line tension and bilayer bending energies.

We note that the geometry of phase-separated budding can be obtained by minimizing an energy functional with contributions from Γ, bending resistance (quantified by κ), total membrane lateral tension σ_{tot}, and normal pressure difference p across the membrane [9,24], see Fig. 5B. The initial situation is a flat circular membrane domain with surface area A and radius $D = (A/\pi)^{1/2}$ giving a total line tension energy $\Gamma = 2\pi D\gamma$ where γ is the line tension energy per unit length. Minimizing the domain circumference and thus Γ can be achieved by transforming the domain into a bud (with surface area A) and neck radius a provided that the energy E to form the bud is less than Γ.

To a first approximation the energy to form the bud can be written as

$$E = \left(\frac{2\kappa}{R^2} + \sigma_{tot}\right)\pi(a^2 + h^2) - p\left(\frac{1}{3}\pi h^2(3R - h)\right), \quad (1)$$

where R is the radius of the budding vesicular cap, h is height of the cap, $\sigma_{tot} = \sigma_{cyt} + \sigma_{mem}$, where σ_{cyt} represents the cytoskeleton adhesion and σ_{mem} the intrinsic membrane tension [24]. A decrease in either σ_{cyt} or σ_{mem} will lower σ_{tot} and potentially destabilize a local domain leading to vesicle fission.

A finite R exists only below a critical value of p and above a critical value of κ [24] and the critical neck radius a_{crit} can be found from:

$$\frac{p a_{crit}}{\sigma_{tot}} = 2 + \frac{8\kappa}{a_{crit}^2 \sigma_{tot}}, \quad (2)$$

We solve Eq. (2) for a_{crit}, and obtain the real-valued solution:

$$a_{crit} = \frac{2\sigma_{tot}}{3p} + \frac{2 \cdot \sqrt[3]{2} \cdot \sigma_{tot}^2}{3p\sqrt[3]{27\kappa p^2 + 2\sigma_{tot}^3 + 3\sqrt{3}\sqrt{27\kappa^2 p^4 + 4\kappa p^2 \sigma_{tot}^3}}} + \frac{\sqrt[3]{2}\sqrt[3]{27\kappa p^2 + 2\sigma_{tot}^3 + 3\sqrt{3}\sqrt{27\kappa^2 p^4 + 4\kappa p^2 \sigma_{tot}^3}}}{3p}. \quad (3)$$

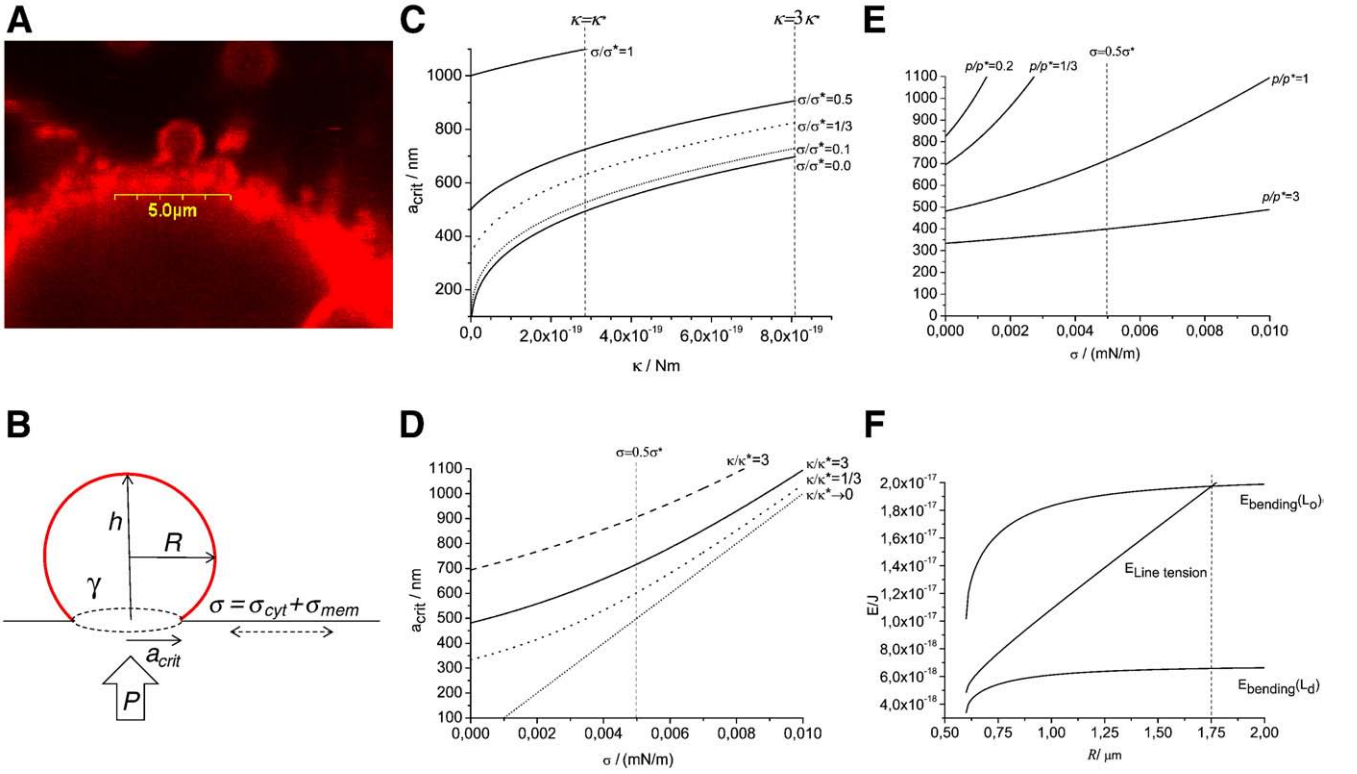

Fig. 5. Line tension drives fission of DiI vesicles. (A) A representative confocal image of a DiI-$C_{18:0}$ stained exocytic vesicle in a cholesterol-depleted-cell (1% MβCD, 30 min, 37 °C), $R=0.90\ \mu m \pm 0.05\ \mu m$, $a=0.67\ \mu m \pm 0.06\ \mu m$ (mean ± sem, $n=7$), (B) Geometry of L_d-like DiI domain (red) vesicle fission from the plasma membrane (black). For symbols, see text. The total line tension Γ is decreased if the domain edge is reduced by the formation of DiI enriched vesicles. (C–F) Analysis of geometry and energetics (Eqs. 1–3) of vesicle budding. Our reference parameters are: $\kappa^*=2.7\ 10^{-19}$ J, $\sigma_{tot}^*=0.005$ mN/m, and $p^*=20$ N/m^2. (C) a_{crit} (κ) for fixed values of σ_{tot}. (D) a_{crit} (σ_{tot}) for fixed values of κ. (E) a_{crit} (σ_{tot}) for fixed values p. (F) $E_{Bending}$ (L_d), $E_{Bending}$ (L_o), and Γ as function of R. Note that $\Gamma > E_{Bending}$ (L_d) for all values of R.

As we demonstrated that MβCD caused a loss of membrane–cytoskeleton adhesion we speculated if the observed budding (and the observed a_{crit}) was consistent with the prediction obtained from Eqs. (1–3).

Therefore we examined how a_{crit} depends on σ_{tot}, κ, and p (Figs. 5C–F). Fig. 5C shows a_{crit} (κ) for different values of σ_{tot} where $\kappa^*=2.7\ 10^{-19}$ J is our reference value for the bending modulus of the L_d phase and $\sigma_{tot}^*=0.01$ mN/m is a reference value for a cell membrane [24]. For a_{crit} to be in the observed range of 400 to 600 nm for $\kappa=\kappa^*$, σ_{tot} must be well below 0.005 mN/m suggesting that σ_{cyt} is significantly reduced. Fig. 5D shows a_{crit} (σ) for different values of κ. For σ_{tot} around 0.005 mN/m we see that κ cannot be vanishingly small as this will lead to too small a_{crit} values. Setting $\kappa=3\kappa^*$ corresponding to a more rigid L_o bilayer [27], a_{crit} becomes too large. Thus $\kappa=\kappa^*$ seems to be a reasonable estimate. Fig. 5E shows that for $\sigma_{tot}=0.005$ mN/m p must be in the order of 20 N/m^2 which is a typical value for the excess pressure, e.g. [28] to fit the observed a_{crit} values.

The observed geometry of vesicle formation can thus be explained using Eq. (3) with reasonable values for κ, σ_{tot} and p. We now compare E for a bud with the total line tension energy $\Gamma=2\pi D\gamma$ for the corresponding flat membrane area where we take $\gamma=0.22$ kT/nm [9] as a reference value. This is shown in Fig. 5F. $E_{Bending}$ (L_d) represents the first term in Eq. (1) (for vanishing p) calculated for $\kappa=\kappa^*$ with $a_{crit}=600$ nm and $\sigma_{tot}=0.005$ mN/m. $E_{Bending}$ (L_o) represents the same with $\kappa=3\kappa^*$. Both curves correspond to the maximal $E_{Bending}$ (as p is neglected). $E_{Bending}$ (L_d)$<\Gamma$ for all values of R. Thus the budding is always favourable. For L_o-like domains budding of vesicles below 1.75 µm will not be energetically favourable. The size of the observed vesicles is consistent with L_d-like domains budding off the cell. Thus cholesterol depletion results in formation of large-scale L_d-like domains with reduced cytoskeletal adhesion (σ_{cyt}). This enables the finite excess internal pressure to yield spontaneous vesicle budding with the dimensions (a_{crit} and R) observed.

4. Discussion

Our data indicate that spontaneous vesiculation of DiI domains occurs in living cells. This is augmented by cholesterol depletion with MβCD, which enhances GM_1/DiI domain separation, detachment of cortical cytoskeleton from the membrane, and reorganization of the subcortical actin meshwork. The exact action of MβCD on cells still remains elusive. In model systems, gel phase sphingomyelin domains surrounded by an L_o matrix rich in cholesterol and 1-palmitoyl-2-oleoyl phosphatidylcholine were observed just before reaching the uniform L_o state. This suggests that raft formation in biological membranes could occur not only via liquid–liquid but also via gel–liquid immiscibility [29].

The current 'raft-hypothesis' postulates that plasma membrane microdomains (rafts) are dynamic 10–200 nm-sized domains. Larger (>200 nm) domains are stabilized by lipid–lipid or lipid–protein interactions under certain conditions [3]. Although µm-scale L_o-domains have been observed in model membranes and µm-scale plasma membrane rafts are normally absent in living cells, µm-scale phase separation has been seen in vesicles derived from rat basophile leukemia mast cell and fibroblast plasma membranes at temperatures below ~25 °C [5]. These vesicles appeared devoid of actin, which could explain the observed large-scale L_o/L_d phase separation.

We demonstrate that it is energetically favourable for L_d-like DiI domains to form vesicles with R and a values comparable to the observations. Although the exact size-estimation is difficult, we note

that if the vesicles were formed mainly from L_o-like domains they would be larger than observed. Our data are compatible with findings [10], which demonstrated that L_d phase lipids are prone to form exocytic tubules from vesicles and that cholesterol perturbation promotes phase separation and tubule fission of the L_d phase [1]. Also the B subunit of shiga toxin can induce lipid reorganization and membrane invaginations potentially driven by line tension [30]. We conclude that Γ is of sufficient magnitude to regulate GM_1/DiI domain separation and L_d-like domain vesicle formation.

We propose that control of membrane budding is realized by cytoskeletal attachments impeding the formation of large-scale L_d-like domains. Loss of (local) attachment may bring smaller L_o-like domains together and create large-scale L_d-like domains, where the lack of attachment enables the cell's internal pressure to bend L_d areas leading to vesiculation. In concordance with results from GUV studies [9], our findings indicate that line tension at the 'L_o/L_d' boundary is a major player in the control of vesicle formation in living cells.

Acknowledgements

We thank Dr. O.S. Andersen, Department of Physiology and Biophysics, Weill Medical College, Cornell University, New York, NY, for helpful comments. We thank Dr. M. Edidin (Biology Department, The John Hopkins University, Baltimore, MD) for providing the PH-GFP plasmid with the permission of Dr. T. Balla (Endocrinology and Reproduction Research Branch, NIH, Bethesda, MD). We thank E. Hoffmann, I. Pedersen and V. Pless for preparation of cell cultures. The Aage Bang Foundation, Danish Society of Dermatology Research Foundation, Bispebjerg Hospital Research Foundation, and Danish National Research Foundation financially supported this work.

References

[1] G. van Meer, Cellular lipidomics, EMBO J. 24 (2005) 3159–3165.
[2] G.W. Feigenson, Phase boundaries and biological membranes, Annu. Rev. Biophys. Biomol. Struct. 36 (2007) 63–77.
[3] L.J. Pike, Rafts defined: a report on the Keystone Symposium on lipid rafts and cell function, J. Lipid Res. 47 (2006) 1597–1598.
[4] A. Kusumi, C. Nakada, K. Ritchie, K. Murase, K. Suzuki, H. Murakoshi, R.S. Kasai, J. Kondo, T. Fujiwara, Paradigm shift of the plasma membrane concept from the two-dimensional continuum fluid to the partitioned fluid: high-speed single-molecule tracking of membrane molecules, Annu. Rev. Biophys. Biomol. Struct. 34 (2005) 351–378.
[5] T. Baumgart, A.T. Hammond, P. Sengupta, S.T. Hess, D.A. Holowka, B.A. Baird, W.W. Webb, Large-scale fluid/fluid phase separation of proteins and lipids in giant plasma membrane vesicles, Proc. Natl. Acad. Sci. U.S. A. 104 (2007) 3165–3170.
[6] T.J. McIntosh, S.A. Simon, D. Needham, C.H. Huang, Structure and cohesive properties of sphingomyelin/cholesterol bilayers, Biochemistry 31 (1992) 2012–2020.
[7] R. Lipowsky, Budding of membranes induced by intramembrane domains, J. Phys. II 2 (1992) 1825–1840.
[8] H.T. McMahon, J.L. Gallop, Membrane curvature and mechanisms of dynamic cell membrane remodelling, Nature 438 (2005) 590–596.
[9] T. Baumgart, S.T. Hess, W.W. Webb, Imaging coexisting fluid domains in biomembrane models coupling curvature and line tension, Nature 425 (2003) 821–824.
[10] A. Roux, D. Cuvelier, P. Nassoy, J. Prost, P. Bassereau, B. Goud, Role of curvature and phase transition in lipid sorting and fission of membrane tubules, EMBO J. 24 (2005) 1537–1545.
[11] N. Kahya, D. Scherfeld, K. Bacia, B. Poolman, P. Schwille, Probing lipid mobility of raft-exhibiting model membranes by fluorescence correlation spectroscopy, J. Biol. Chem. 278 (2003) 28109–28115.
[12] K. Bacia, D. Scherfeld, N. Kahya, P. Schwille, Fluorescence correlation spectroscopy relates rafts in model and native membranes, Biophys. J. 87 (2004) 1034–1043.
[13] T. Baumgart, G. Hunt, E.R. Farkas, W.W. Webb, G.W. Feigenson, Fluorescence probe partitioning between Lo/Ld phases in lipid membranes, Biochim. Biophys. Acta 1768 (2007) 2182–2194.
[14] C. Gomez-Mouton, R.A. Lacalle, E. Mira, S. Jimenez-Baranda, D.F. Barber, A.C. Carrera, C. Martinez-A, S. Manes, Dynamic redistribution of raft domains as an organizing platform for signaling during cell chemotaxis, J. Cell Biol. 164 (2004) 759–768.
[15] A.T. Hammond, F.A. Heberle, T. Baumgart, D. Holowka, B. Baird, G.W. Feigenson, Crosslinking a lipid raft component triggers liquid ordered–liquid disordered phase separation in model plasma membranes, Proc. Natl. Acad. Sci. U. S. A. 102 (2005) 6320–6325.
[16] D. Vind-Kezunovic, U. Wojewodzka, R. Gniadecki, Focal junctions retard lateral movement and disrupt fluid phase connectivity in the plasma membrane, Biochem. Biophys. Res. Commun. 365 (2008) 1–7.
[17] P. Boukamp, R.T. Petrussevska, D. Breitkreutz, J. Hornung, A. Markham, N.E. Fusenig, Normal keratinization in a spontaneously immortalized aneuploid human keratinocyte cell line, J. Cell Biol. 106 (1988) 761–771.
[18] P. Varnai, T. Balla, Visualization of phosphoinositides that bind pleckstrin homology domains: calcium- and agonist-induced dynamic changes and relationship to myo-[^{3}H]inositol-labeled phosphoinositide pools, J. Cell Biol. 143 (1998) 501–510.
[19] R. Gniadecki, B. Gajkowska, J. Bartosik, M. Hansen, H.C. Wulf, Variable expression of apoptotic phenotype in keratinocytes treated with ultraviolet radiation, ceramide, or suspended in semisolid methylcellulose, Acta Derm. Venereol. 78 (1998) 248–257.
[20] J.A. Nickerson, G. Krochmalnic, S. Penman, Isolation and visualization of the nuclear matrix, the nonchromatin structure of the nucleus, in: J.E. Celis (Ed.), Cell Biology: A Laboratory Handbook, vol. 2, Academic Press, San Diego, 1998, pp. 184–192.
[21] R. Gniadecki, H. Olszewska, B. Gajkowska, Changes in the ultrastructure of cytoskeleton and nuclear matrix during HaCaT keratinocyte differentiation, Exp. Dermatol. 10 (2001) 71–79.
[22] R. Gniadecki, B. Gajkowska, Detection of cytomatrix proteins by immunogold embedment-free electron microscopy, in: J.R. Harris, J.M. Graham, J. Rickwood (Eds.), Cell Biology Protocols, J. Wiley and Sons, Chichester, UK, 2006, pp. 317–325.
[23] T. Harder, P. Scheiffele, P. Verkade, K. Simons, Lipid domain structure of the plasma membrane revealed by patching of membrane components, J. Cell Biol. 141 (1998) 929–942.
[24] M.P. Sheetz, J.E. Sable, H.G. Dobereiner, Continuous membrane–cytoskeleton adhesion requires continuous accommodation to lipid and cytoskeleton dynamics, Annu. Rev. Biophys. Biomol. Struct. 35 (2006) 417–434.
[25] H.L. Yin, P.A. Janmey, Phosphoinositide regulation of the actin cytoskeleton, Annu. Rev. Physiol. 65 (2003) 761–789.
[26] J. Kwik, S. Boyle, D. Fooksman, L. Margolis, M.P. Sheetz, M. Edidin, Membrane cholesterol, lateral mobility, and the phosphatidylinositol 4,5-bisphosphate-dependent organization of cell actin, Proc. Natl. Acad. Sci. U. S. A. 100 (2003) 13964–13969.
[27] D. Needham, R.S. Nunn, Elastic deformation and failure of lipid bilayer membranes containing cholesterol, Biophys. J. 58 (1990) 997–1009.
[28] J. Dai, M.P. Sheetz, Membrane tether formation from blebbing cells, Biophys. J. 77 (1999) 3363–3370.
[29] M.C. Giocondi, P.E. Milhiet, P. Dosset, C. Le Grimellec, Use of cyclodextrin for AFM monitoring of model raft formation, Biophys. J. 86 (2004) 861–869.
[30] W. Romer, L. Berland, V. Chambon, K. Gaus, B. Windschiegl, D. Tenza, M.R.E. Aly, V. Fraisier, J.-C. Florent, D. Perrais, C. Lamaze, G. Raposo, C. Steinem, P. Sens, P. Bassereau, L. Johannes, Shiga toxin induces tubular membrane invaginations for its uptake into cells, Nature 450 (2007) 670–675.